THE JOURNAL OF PHYSICAL CHEMISTRY B
A JOURNAL OF THE AMERICAN CHEMICAL SOCIETY

pubs.acs.org/JPCB

Article

Dynamics of Acrylamide Hydrogels, Polymers, and Monomers in Water Measured with Optical Heterodyne-Detected Optical Kerr Effect Spectroscopy

Stephen J. Van Wyck and Michael D. Fayer*

Cite This: *J. Phys. Chem. B* 2023, 127, 1276−1286

Read Online

ACCESS | Metrics & More | Article Recommendations | Supporting Information

ABSTRACT: The ultrafast dynamics of acrylamide monomers (AAm), polyacrylamide (PAAm), and polyacrylamide hydrogels (PAAm-HG) in water were studied using optical heterodyne-detected optical Kerr effect (OHD-OKE) spectroscopy. Previous ultrafast infrared (IR) measurements of the water dynamics showed that at the same concentration of the acrylamide moiety, AAm, PAAm, and PAAm-HG exhibited identical water dynamics and that these dynamics slowed with increasing concentration. In contrast to the IR measurements, OHD-OKE experiments measure the dynamics of both the water and the acrylamide species, which occur on different time scales. In this study, the dynamics of all the acrylamide systems slowed with increasing concentration. We found that AAm exhibits tetraexponential decays, the longest component of which followed Debye−Stokes−Einstein behavior except for the highest concentration, 40% (w/v). Low concentrations of PAAm followed a single power law decay, while high concentrations of PAAm and all concentrations of PAAm-HG decayed with two power laws. The highest concentrations, 25% and 40%, of PAAm and PAAm-HG showed nearly identical dynamics. We interpreted this result as reflecting a similar extent of chain−chain interactions. At low concentrations, PAAm displays non-Markovian, single-chain dynamics (single power law), but PAAm displays entangled chain−chain interactions at high concentrations (two power laws). PAAm-HG has chain−chain interactions at all concentrations that arise from the cross-linking. At high concentrations, the dynamics of the entangled of PAAm become identical within error as those of the cross-linked PAAm-HG.

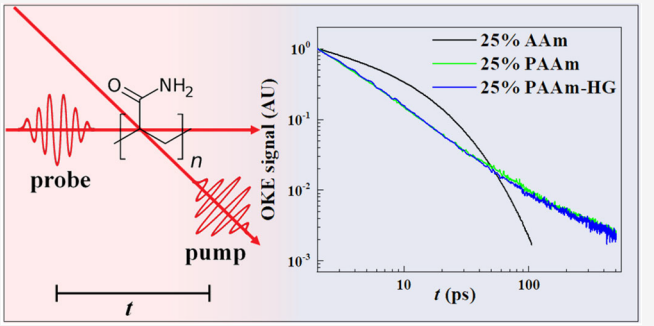

I. INTRODUCTION

Hydrogels are polymer semirigid networks that can incorporate large amounts of water into their structure. Microscale pores are formed by cross-linking polymer chains, and these pores are preserved when the polymer is swollen by water. The pores give rise to materials that are permeable to gases and macromolecule solutes.[1,2] These characteristics make hydrogels useful in applications for contact lenses,[3] tissue engineering,[4,5] and other biomedical applications.[6−8] Polyacrylamide hydrogels in particular have been vital in the development of these technologies. The ability to tune the size of the pores by varying the mass fraction of polymer has led to the widespread use of polyacrylamide hydrogels for gel permeation chromatography,[9] electrophoresis,[10,11] and as a culture substrate.

Water makes up most of the polyacrylamide hydrogel and plays a large role in its properties. Hydrogen bonds (H-bonds) between polymer acrylamide moieties and water and non-hydrogen bonded water molecules in the first solvation of the polymer greatly affect the polymer's structure and dynamics.[12] In bulk water, there are two time scales observed in ultrafast two-dimensional infrared (2D IR) measurements of the H-bond network dynamics, a fast component (∼400 fs) due to local H-bond fluctuations of the intact H-bond network and a slower 1.7 ps component attributed to complete randomization of the H-bond network.[13−18] Simulations show that water molecules not in the first solvation shell of the acrylamide polymer or monomer behave as bulk water.[19] The addition of more solute into the water reduces the amount of bulk water. The simulation demonstrates that water molecules in the first solvation shell display very different dynamics from those of bulk water.[20]

Experiments on polyacrylamide hydrogels using time-resolved fluorescence and ultrafast IR have also been reported. Time-resolved fluorescence employed a large aromatic fluorescent molecule; the measurements were limited to observing relatively slow dynamics.[21,22] Ultrafast IR studies have directly monitored the dynamics of the water

Received: November 21, 2022
Revised: January 17, 2023
Published: January 27, 2023

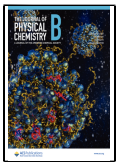

https://doi.org/10.1021/acs.jpcb.2c08164
J. Phys. Chem. B 2023, 127, 1276−1286

molecules.[19,20,23] An early study reported that water dynamics in the cross-linked polyacrylamide hydrogels slowed with increasing hydrogel concentrations.[23] This slowing was ascribed to the decrease of the pore sizes, leading to increased confinement. A later ultrafast IR study found that the water dynamics were identical for acrylamide, polyacrylamide, and cross-linked polyacrylamide hydrogels, when the concentration of acrylamide moieties was held constant.[19] Another ultrafast IR study found that water dynamics were identical in solutions of poly-*N*-isopropylacrylamide and *N*-isopropylacrylamide.[20] As there is a limited confinement effect for acrylamide and polyacrylamide, the mechanism for slowing dynamics was amended to arise from interactions of the water with individual acrylamide moieties. Optical heterodyne-detected Raman-induced Kerr effect spectroscopy (OHD-RIKES) is another ultrafast technique that has been used to study aqueous polyacrylamide solutions.[24] Aqueous propionamide was also studied as a model of the repeating unit of polyacrylamide. Biexponential decays were observed with a fast time constant on the order of 1 ps and the slower time constant ranging from 4 to 10 ps. It was found that the dynamics of both polyacrylamide and propionamide scaled linearly with concentration despite large differences in the viscosity scaling. The experimental setup limited the experimental time to range to ∼35 ps, which prevented the observation of slower decay processes.

Here, we present optical heterodyne-detected optical Kerr effect (OHD-OKE) experimental studies of acrylamide monomers (AAm), polyacrylamide (PAAm), and cross-linked polyacrylamide hydrogel (PAAm-HG). OHD-OKE experiments are similar to OHD-RIKES. However, implementation of OHD-OKE enables dynamics to be studied from subpicosecond to 500 ps time scales, which cover the full range of dynamics. In contrast to ultrafast IR experiments on these acrylamide systems, OHD-OKE reports principally on the dynamics of the acrylamide polymers and monomers although fast water dynamics are also observed.

Of particular importance is the observation of polymer chain dynamics and the major differences between the PAAm and PAAm-HG as a function of concentration. Both the polymers and hydrogels display fundamentally different dynamics than the acrylamide monomers. The monomers' OHD-OKE data decay as concentration-dependent tetraexponentials. The slowest exponent component obeys the Stokes−Einstein-Debye equation for orientational relaxation except at the highest concentration, 40%. In contrast, the PAAm and PAAm-HG OHD-OKE data are power law decays. The power laws reflect non-Markovian chain dynamics. At low concentrations, the PAAm data are single power laws, while at the same concentrations, the PAAm-HG data decay as two power laws. At high concentrations, the PAAm decays as two power laws, and the data become virtually the same as the PAAm-HG decays. These behaviors are attributed to chain−chain interactions. The OHD-OKE experiments provided a detailed picture of the dynamics of the three types of acrylamide systems and the roles of polymerization and cross-linking.

II. EXPERIMENTAL PROCEDURES

II.A. Sample Preparation and Viscosity Measurements. Acrylamide was purchased from Sigma-Aldrich with a greater than 99% purity and used as received. Solid acrylamide was dissolved in deionized water to make solutions of a known concentration (AAm). The acrylamide mass concentrate was reported as a percentage of the weight of acrylamide (g) over the volume (mL) of the solution (w/v). The concentration was varied from 5% to 40%. The viscosity of AAm was measured using Cannon-Ubbelohde viscometry. PAAm was prepared by polymerizing AAm using ammonium persulfate (10 μL of 10% in water) as an initiator and *N*,*N*,*N*′,*N*′-tetramethylethylenediamine (1 μL) as a catalyst. To prepare PAAm-HG, a proportion of the acrylamide in the precursor solutions was replaced by a cross-linker, *N*,*N*′-methylenebis(acrylamide) (abbreviated bis). The percentage of bis in the polymer mass was 3.3%. PAAm-HG was polymerized in the same manner as PAAm. PAAm and PAAm-HG were allowed to polymerize overnight or longer. The solutions were syringe filtered (0.022 μm) and transferred to an optical grade 1 cm cuvette. All experiments were performed at 24.4 °C.

II.B. Optical Kerr Effect Setup. The OHD-OKE experiment is a nonresonant, pump−probe technique that measures the orientational dynamics of condensed materials, without the use of molecular probes. When the intense, polarized pump-pulse is incident on the analyte, the molecules' configurations are no longer random but rather are minutely aligned relative to the pulse's electric field. The alignment and resulting birefringence will decay due to the random motions of the molecules. The resulting signal is the time derivative of the polarizability-polarizability correlation function. For the two types of polymers, the equilibrium distribution of chain structures is perturbed by the electric field. Acrylamide moieties, short chain segments, side groups, etc. will respond to the electric field producing an ensemble polarizability anisotropy. Relaxation of the perturbed chain structures through random motion will occur such that the final ensemble is no longer an ensemble anisotropy polarization. A particular perturbed structure does not necessarily return to the original configuration it had prior to the pump pulse. Rather, through the relaxation of the individual polymer structural subunits, the ensemble of polymers will return to a thermal equilibrium configuration. This configuration, like the starting configuration, will be isotropic and will not give rise to a birefringence. The nature of the polymer relaxation will be discussed in detail below.

The OHD-OKE setup has been described thoroughly elsewhere.[25,26] Briefly, short pulses were produced using a Ti-Sapphire oscillator. The power of these pulses was increased using a regenerative amplifier operating at a 5 kHz repetition rate. This resulted in pulses of as short as ∼80 fs with an energy of 0.2 mJ. These pulses were split with a (98%)/(2%) beam splitter to produce intense pump and weaker probe pulses. The pump arrived at the sample linearly polarized at ±45° relative to the probe. The polarization was switched between the two 45° polarizations at 1.25 kHz with a Pockels cell, which provided phase cycling. The arrival time of the probe was scanned with a stepper delay stage. For greater detection sensitivity, heterodyne detection was used. Another Pockels cell introduced a slight (±3°) ellipticity to the probe pulse at 2.5 kHz. This resulted in a collinear local oscillator, which provided heterodyne detection. In addition, the heterodyned signal beam and a reference beam were measured with a photodiode-balanced detector that removed most of the local oscillator. Combining the polarization alternation, the phase cycling, and the balanced detection provided exceptional signal-to-noise. Because the OKE is a nonresonant optical property of the material, the technique was not dependent on

https://doi.org/10.1021/acs.jpcb.2c08164
J. Phys. Chem. B 2023, 127, 1276−1286

using a probe molecule or limited by an excited state lifetime. OHD-OKE observed the system's thermal equilibrium ground state dynamics.

The OHD-OKE signal was analyzed with several different functions depending on the system. The water and AAm data were fit with a multiexponential function. In contrast, the PAAm and PAAm-HG solutions were analyzed with a method that is commonly employed in schematic mode coupling theory (MCT) analysis of OHD-OKE supercooled liquid dynamics data[27−30] and similar systems.[31−33] The numerical solutions to MCT's coupled differential equations have been modeled by one or more power laws followed by a final exponential. The final exponential reflects the complete randomization of the small molecule liquid systems. This final exponential decay, however, was not observed in data for PAAm and PAAm-HG as complete randomization of the solutions of long chain length polymers would take place over extremely long time scales. The power law decays extend to <0.1% of the original signal, indicating that a negligible or zero component of the signal arises from changes in the overall configurations of the entire system of polymers. These experiments are somewhat akin to previous OHD-OKE studies of the nematic phase-aligned liquid crystals.[34,35] The excitation pulse moves the system away from the thermal equilibrium order parameter, and the signal decay reflects relaxation back to the original order parameter rather than randomization of the liquid crystal structure. As discussed below, the 5% and 10% PAAm fit well to a single power function except at very short times. A fast exponential decay was used to capture water dynamics. For higher concentration PAAm and all PAAm-HG samples, two power laws were required to fit the data. The data make a smooth transition from the first power law decay, t^{-a} to t^{-b}. The fitting function, eq 1, allows the time and temporal width of the transition to be included in the fit.

$$R(t) = A_1\exp(-t/\tau) + \frac{A_2}{2}\left[1 - \mathrm{erf}\left(\frac{\ln(t) - n}{\sqrt{2}\,u}\right)\right]t^{-a} + \frac{A_3}{2}\left[1 + \mathrm{erf}\left(\frac{\ln(t) - n}{\sqrt{2}\,u}\right)\right]t^{-b} \quad (1)$$

The error functions essentially turn off the first power law, while turning on the second. The parameters n and u determine where the transition is centered and its width, respectively. Eq 1 ensured that the power laws do not bleed into each other. Each power law was initially fit over an appropriate time range. These power law exponents were used as initial parameters for fitting the entire decay using eq 1.

III. RESULTS AND DISCUSSION

III.A. Source of the OHD-OKE Signal. At relevant time scales (long compared to the pulse duration), the OHD-OKE signal is the time-derivative of the polarizability-polarizability correlation function.[36−38] Any molecules that possess an anisotropic polarizability will contribute to the signal, but the strength of the signal will depend on the magnitude of the polarizability anisotropy. OHD-OKE does not have the specificity to distinguish between relative water and analyte contributions to the overall decay.

Water has been previously reported as having a relatively weak anisotropic polarizability.[39−42] Electronic calculations of water, AAm, and acrylamide dimer oligomer (2AAm) were performed. The computational details are given in the Supporting Information (SI). The calculations for single isolated molecules give the AAm signal ∼500 times larger than water. However, water exists as a hydrogen-bonded network; therefore, it is not certain exactly what the relative sizes of the signals will be. Some of the water molecules are in the first solvation shell of the AAm, and these may not have the same polarizability anisotropy as the water outside the first solvent shell. From ultrafast IR experiments[20] and molecular dynamics (MD) simulations,[19] water outside the first solvent shell behaves essentially like bulk water. In addition, the water concentration is much higher than the AAm concentration, particularly at the lower concentrations. Therefore, it is not surprising that we observe a signal from water as well as AAm. However, as discussed below, the water dynamics are very fast, so, at longer times, the signal is exclusively from the AAm. Even at the lowest acrylamide concentrations, it can be assumed that the long-time signal is primarily arising from acrylamide. Figure 1 shows the data for the pure water and for AAm at four concentrations normalized at t = 1 ps. Water dynamics in the AAm solutions are similar to those of bulk water (see below).

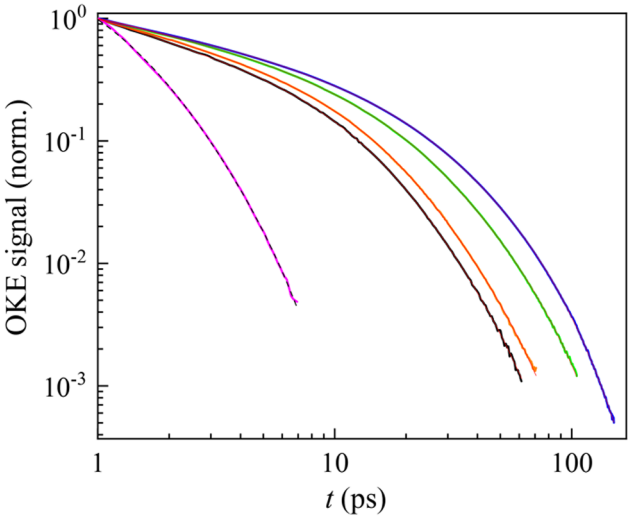

Figure 1. OHD-OKE decays of water (purple) and 5% (black), 10% (orange), 25% (green), and 40% (blue) AAm in water. Spectra were normalized at 1 ps. The dashed lines are biexponential and tetraexponential fits for water and AAm solutions, respectively. The decays slow down with increased AAm concentration.

Providing an estimate of the polarizability anisotropy of polyacrylamide presents more challenges. It is not computationally feasible or informative to perform calculations of a larger polyacrylamide chain. Other studies have suggested that polyacrylamide's signal is less than 10% of AAm.[24] In the effort to get a closer approximation of polyacrylamide, polarizability anisotropy of 2AAm was calculated. For each acrylamide moiety, the signal of 2AAm was 43 times larger than that of a single water molecule. It was determined that the calculations could not be meaningfully extended to large oligomers. Therefore, due to water's abundance in the solution, it contributes to the PAAm and PAAm-HG solution signals but only at relatively short times.

III.B. OHD-OKE of Water and Acrylamide (AAm) in an Aqueous Solution. The OHD-OKE decays were collected for bulk water and four concentrations of AAm in water (see

https://doi.org/10.1021/acs.jpcb.2c08164
J. Phys. Chem. B 2023, 127, 1276−1286

Table 1. Viscosity and Parameters for Multiexponential for Water and AAm

concn (w/v)	vis (cP)	t_1(ps)[a]	t_2(ps)[a]	t_3(ps)[b]	t_4(ps)[b]	C_1 norm	C_2 norm	C_3 norm	C_4 norm
water	0.91	0.52 ± 0.03	1.29 ± 0.02	n/a	n/a	0.83 ± 0.01	0.17 ± 0.01	n/a	n/a
5%	1.00	0.52[c]	1.70 ± 0.07	6.0 ± 0.3	14.1 ± 0.8	0.54 ± 0.02	0.20 ± 0.02	0.22 ± 0.01	0.037 ± 0.004
10%	1.11	0.52[c]	1.90 ± 0.22	6.9 ± 0.4	16.2 ± 1.7	0.50 ± 0.05	0.22 ± 0.03	0.24 ± 0.01	0.04 ± 0.01
25%	1.52	0.52[c]	2.56 ± 0.11	9.4 ± 0.2	22.9 ± 0.4	0.51 ± 0.01	0.23 ± 0.01	0.21 ± 0.01	0.05 ± 0.01
40%	2.09	0.52[c]	2.53 ± 0.05	10.3 ± 0.3	25.7 ± 0.7	0.50 ± 0.01	0.23 ± 0.01	0.19 ± 0.01	0.09 ± 0.01

[a]Parameters for water not associated with the polymer. [b]Acrylamide (AAm) monomer parameters. [c]Parameter fixed to the bulk number value as it is essentially constant in the fits.

Figure 1). The concentration was varied from 5% to 40% (w/v). All the decays were fit to a multiexponential function (Table 1). Pure water was found to fit well to a biexponential, which is consistent with other dynamics of measure of water.[19,23,39,42] Lifetime density analysis has been previously employed to evaluate the validity of models (Figure S1).[43] It was found that water and all AAm concentration share fast time components, and AAm solutions can be modeled well as a tetraexponential. The two fastest components (t_1 and t_2) are assigned to water dynamics. The two slower time decays (t_3 and t_4) arise from the orientational relaxation of AAm.

The biexponential fit to pure water yields time constants, t_1 = 0.52 ± 0.03 ps and t_2 = 1.29 ± 0.02 ps. These values are similar to time scales measured for water dynamics with 2D IR experiments, i.e., 0.4 ± 0.05 ps and 1.7 ± 0.1 ps.[19] MD simulations of the 2D IR showed that the faster value arises from very local H-bond fluctuations, mainly length fluctuations, while the second value reflects the complete randomization of the H-bond network.[19] However, the two experiments measure fundamentally different correlation functions. 2D IR measures the frequency-frequency correlation function of the hydroxyl stretch, while OHD-OKE measures the polarizability-polarizability correlation function. Nonetheless, it is possible that the processes assigned by the MD simulations are also responsible for the decays observed with OHD-OKE experiments.

The water present in AAm can be divided into two populations, bulk and surface water. Surface water refers to water present in the first solvation shell of AAm. The fast behavior of both populations is believed to be the same. Previous FT-IR studies have shown that HOD's OD stretch changes little in solutions of AAm in dilute HOD/H_2O as a function of AAm concentration. Bulk water and 25% AAm have essentially the same FT-IR spectrum, indicating that water and acrylamide have similar H-bond strengths.[19,20] The similar H-bonds environments will yield H-bond fluctuation dynamics that will deviate little from pure water. With this knowledge and to ensure convergence, the fastest component was fixed to t_1 = 0.52 ps, which is the same as water. The second component ranges from t_2 = 1.70 ± 0.07 ps to t_2 = 2.56 ± 0.11 ps becoming longer as the AAm concentration increases. This component reflects the complete randomization of water's H-bond network, which is slowed by its interactions with AAm. Previous ultrafast IR anisotropy data showed that bulk and surface waters have orientational relaxations with distinct time scales,[19,20] for the orientational relaxation responsible for H-bond randomization. OKE−OHD is unable to distinguish the two water populations. Therefore, both populations will be present in the slowest component, t_2, of the water relation data.

To help elucidate the water dynamics, the acrylamide time components (t_3 and t_4) were subtracted out from the data (Figure S2). The water data after subtraction fits well to a biexponential with the first time constant fixed to water's fast component, 0.52 ps, and the second time constant allowed to float. The second time constant has the same value as the t_2 from tetraexponential fits of the full data. While the water data after subtraction can be fit as a biexponential, by using a triexponential, we can determine the populations of bulk and surface waters. The first time constant remains the same, 0.52 ps. The second time constant is fixed to the complete H-bond network randomization of bulk water, 1.29 ps. The third time constant is fixed to 2.6 ps, which reflects the dynamics of surface water. It is approximately the value of t_2 for 25% and 40% AAm. At the high concentration, there are only six waters per acrylamide. Other studies have found that far more than six waters are required to solvate acrylamide, which means there is ample sharing between the solvation shells of 40% AAm, and no bulk water is present.[19,44] With the time constants fixed, only the amplitudes of the two components are varied, with their sum having to equal the total amplitude of the t_2 component. This ratio of the bulk and surface components' amplitudes permits the number of surface waters per acrylamide to be determined. The details of the analysis are given in the Supporting Information. For 5% AAm and 10% AAm, there are 18 and 15 surface waters per acrylamide, respectively. This is consistent with values from previous studies.[19,44] At high concentrations, 25% AAm and 40% AAm, it was determined that basically all the waters were on the surface of the acrylamide, and there was very little or no bulk water. The decay of the water component fits only to the 0.52 ps and 2.6 ps components. The 1.29 ps component was absent. This result is consistent with the limited number of waters per acrylamide, only 12 and 6 for 25% AAm and 40% AAm, respectively.

While the fastest two components of the decay arise from water orientational dynamics, the slowest two components are from acrylamide orientational relaxation. It was found that the slowest time constant (t_4) for 5% to 25% AAm followed the generalized Stokes−Einstein-Debye (SED) equation given in eq 2

$$\tau_{self} = \frac{\eta(T) V f_\theta I_c}{k_B T} \tag{2}$$

where τ_{self} is the single-molecule rotational self-diffusion time, $\eta(T)$ is the temperature-dependent shear viscosity, V is the solvent excluded volume, f_θ is the shape factor to account for divergence from spherical, I_c is an interaction that varies from 0 to 1 depending on interaction with neighboring molecules, k_B is the Boltzmann constant, and T is the absolute temperature.[45−48] Based on the interactions typical for a solute surrounded by smaller solvent molecules, stick boundary conditions are assumed, which means I_c = 1. The solvent

https://doi.org/10.1021/acs.jpcb.2c08164
J. Phys. Chem. B 2023, 127, 1276−1286

excluded volume was 58 Å^3 with an f_θ of 1.15. The viscosity was measured for each solution. Figure 2 shows the slow time

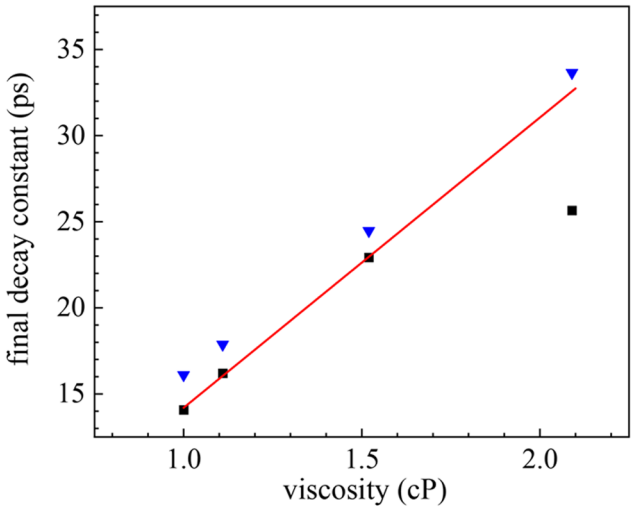

Figure 2. Final exponential decays of AAm versus viscosity in black squares. The data can be found in Table 1. The red line is a linear fit through the first three black squares. The blue triangles are the DSE predictions of the time constants.

constant (t_4) versus viscosity in black squares. The red line is a linear fit through 5% to 25% AAm and extends to 40%. The blue triangles are the predicted time constants based on SED (eq 2) with no adjustable parameters. The SED calculations yield remarkably good predictions up to 25% AAm. At 40% AAm, the dynamics are significantly faster than predicted by the SED equation. At the highest concentration, there are only 6 water molecules per acrylamide. Previous research and results discussed above indicate that ~14 water molecules are required to solvate an acrylamide.[44] Therefore, at 40% AAm, there is considerable sharing of water molecules among the first solvate shells of different acrylamides. This sharing contributes to an increase in viscosity but does not slow the dynamics to the extent predicted by the SED hydrodynamic theory. Previous OKE experiments on propionamide showed similar behavior as the AAm presented here,[24] but the data did not cover the large time range of the current experiments.

As the slowest component for 5% to 25% AAm scales with viscosity and shows hydrodynamic behavior, it is assumed there are limited collective motions contributing to the OHD-OKE polarizability-polarizability correlation function; then, the dynamics are described by $C_2(t)$, the single molecule second-order Legendre polynomial orientational correlation function.[49] As discussed above, OHD-OKE is the derivate of the polarizability-polarizability correlation function. Therefore, the exponential fits were integrated and normalized to 1 at $t = 0$,[26] yielding the following expression

$$C_2(t) = A_{in} + (1 - A_{in})\left[\left(\frac{t_3C_3}{t_3C_3 + t_4C_4}\right)\exp\left(-\frac{t}{t_3}\right) + \left(\frac{t_4C_4}{t_3C_3 + t_4C_4}\right)\exp\left(-\frac{t}{t_4}\right)\right]$$

$$A_3 = (1 - A_{in})\left(\frac{t_3C_3}{t_3C_3 + t_4C_4}\right)$$

$$A_4 = (1 - A_{in})\left(\frac{t_4C_4}{t_3C_3 + t_4C_4}\right) \quad (3)$$

where A_{in} is the amplitude of the inertial component. The inertial component represents femtosecond dynamics that are often too fast for most laser systems to observe. The values of the other parameters can be found in Table 1. OHD-OKE cannot determine the amplitude of the inertial component. IR time-resolved polarization selective pump−probe experiments obtain $C_2(t)$ by multiplying the measured IR anisotropy decay data by 2.5. The inertial component can be obtained from the difference from 1 of the data extrapolated to $t = 0$. Typically, the inertial component ranges from 0.075 to 0.175, but it is frequently close to 0.1. For the purposes of this analysis, A_{in} = 0.1 was chosen, but as shown below, the following analysis is not very sensitive to this choice.[19,50−54]

The observed biexponential behavior of acrylamide can be described using the wobbling-in-a-cone model.[55−57] In this model, there are two diffusion processes following the ultrafast inertial motions. First, the molecule diffuses within a cone with half angle θ. Second, the slower complete orientational relaxation occurs. {The wobbling model has been used to describe biexponential or multiexponential orientational relaxation in a wide variety of isotropic liquids when the probe molecule is of similar size and sometimes larger than the solvent. This includes $SeCN^-$ in ionic liquids, guanidinium in aqueous salt solutions, and water in concentrated LiCl water solutions.[52,58,59]} A system that is very close to the one discussed here is $SeCN^-$ in water.[60] Although $SeCN^-$ is substantially larger than water, the anisotropy decay is biexponential. Detailed MD simulations were able to accurately reproduce the anisotropy decay data. The feature that resulted in $SeCN^-$ displaying wobbling-in-a-cone behavior was the fact that it formed multiple hydrogen bonds with water. Acrylamide also forms multiple H-bonds. It is both a donor and an acceptor. Like SCN^-, these multiple H-bonds restrict acrylamide's orientational relaxation on a shorter time scale.

With this wobbling model, $C_2(t)$ is described in the following manner[61]

$$C_2(t) = (1 - A_{in})\left[S^2 + (1 - S^2)\exp\left(\frac{-t}{\tau_c}\right)\right]\exp\left(\frac{-t}{\tau_m}\right) \quad (4)$$

where S^2 is the order parameter that describes the degree of restriction of the diffusive cone wobbling. An order parameter of 0 is unrestricted reorientation, and 1 is for a cone of 0 angular width. τ_c is the wobbling-in-the-cone time constant for diffusive sampling of the limited range of angles. Finally, τ_m is the final diffusive full orientational relaxation time constant. τ_m is equal to t_4. τ_c can be determined from t_3 and t_4 using the relation

$$\tau_c = (t_3^{-1} + t_4^{-1})^{-1} \quad (5)$$

https://doi.org/10.1021/acs.jpcb.2c08164
J. Phys. Chem. B 2023, 127, 1276−1286

The combination of the inertia cone and the diffusive cone reflects the total angular sampling prior to relaxation of constrains that permits full orientational randomization of the acrylamides.

The cone half angle of interest is the total cone, which is a combination of the inertial and diffusive cones. The cumulative order parameter for the total cone is found through $S_{tot}^2 = (1-A_{in})^2 S^2$, which is equal to A_4 from eq 3.[62] The cumulative order parameter is related to the total cone half angle, θ_{tot}, through the following equation

$$S_{tot} = \frac{1}{2}\cos\theta_{tot}(1 + \cos\theta_{tot}) \quad (6)$$

The parameters found from the wobbling-in-a-cone analysis are given in Table 2.

Table 2. Wobbling-in-a-Cone Time Constants and Total Cone Angle

concn (w/v)	τ_c(ps)	τ_m(ps)	θ_{tot}
5%	4.2	14.1	51°
10%	4.8	16.2	51°
25%	6.7	22.9	46°
40%	7.4	25.7	39°

The choice of possible values of A_{in} had little effect on θ_{tot}. When the analysis is done using $A_{in} = 0.2$, θ_{tot} is increased by a couple of degrees. When the analysis is done with $A_{in} = 0.05$, the angles decrease by less than one degree. Therefore, our choice of $A_{in} = 0.1$ has little impact on the final analysis.

Wobbling-in-a-cone time constants for 5% and 10% AAm are similar in magnitude and have identical total cone angles, 51°. This indicates they are in similar solvent environments with only a minor difference due to differing viscosities. From the discussion above, at low concentration AAm has ample water available to solvate the acrylamides. As acrylamide concentrations increase, the time constants increase, while the cone angles decrease, becoming 46° for 25%. Acrylamide's motion becomes more restricted as indicated by a smaller range of angles sampled. It should be noted that while a cone angle is given for 40% AAm, the wobbling-in-a-cone analysis may not apply because there is a significant deviation from SED behavior.

III.C. OHD-OKE of Polyacrylamide (PAAm) in an Aqueous Solution. Previous ultrafast IR studies have examined the dynamics of water in polymer solutions.[19,20,23] Similar studies to those presented here have interrogated the dynamics of the polymers over a limited time range.[24] Figure 3 shows the OHD-OKE decays of the PAAm in water over the full time range of the observable dynamics. Data were collected for concentrations from 5% to 40% (w/v). It was found that 5% and 10% PAAm fit remarkably well to a fast exponential plus a single power law

$$R(t) = A_1 \exp\left(-\frac{t}{\tau}\right) + A_2 t^{-a} \quad (7)$$

For the higher concentrations, 25% and 40%, the first 100 ps fit well to eq 7, but after ~100 ps, a second slower power law was observed. The phenomenological fitting function (eq 1) allows for switching between the two power law regimes. For both power law models (eqs 1 and 7), the fast exponential captures the dynamics of bulk and surface water as discussed above for acrylamide monomers. The water decay is less evident than in

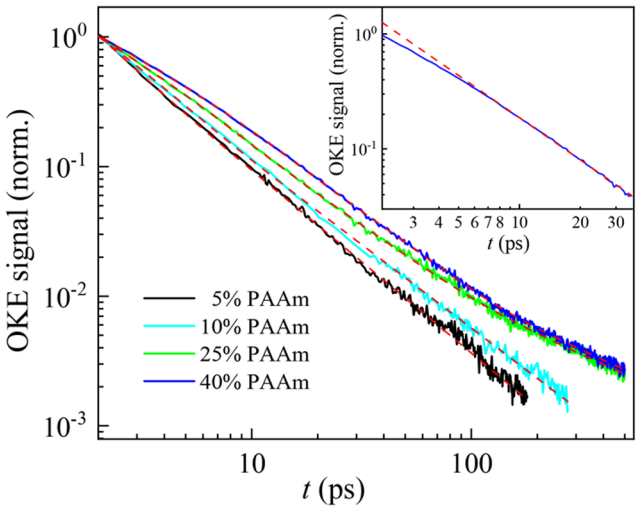

Figure 3. OHD-OKE decays of 5% (black), 10% (teal), 25% (green), and 40% (blue) PAAm in water. Decays were normalized at 2 ps. Red dashed lines are eq 7 fits for 5% and 10% PAAm and eq 1 fits for 25% and 40% PAAm. The inset shows 40% PAAm with a single power law fit. The decays slow down with increased PAAm concentration.

AAm, so a single exponential captures the water dynamics. Without accounting for the short time exponential decay of the water relaxation, the power law misses the data as shown in the Figure 3 inset, which is the early time data for 40% PAAm. The dynamic parameters are given in Table 3. The water dynamics

Table 3. Power Law Fit Exponents for PAAm (Polymer) and PAAm-HG (Cross-Linked Polymer)

concn (w/v)	a	b	τ (ps)
	PAAm		
5%	1.41 ± 0.05	n/a	1.0 ± 0.1
10%	1.29 ± 0.06	n/a	1.7 ± 0.9
25%	1.14 ± 0.02	0.79 ± 0.02	3.1 ± 0.5
40%	1.08 ± 0.02	0.78 ± 0.02	5.5 ± 0.8
	PAAm-HG		
5%	1.67 ± 0.04	0.86 ± 0.05	0.7 ± 0.1
10%	1.43 ± 0.05	0.79 ± 0.05	0.8 ± 0.1
25%	1.14 ± 0.04	0.80 ± 0.02	3.5 ± 0.5
40%	1.07 ± 0.03	0.75 ± 0.04	5.8 ± 0.8

can be fit with 1 ps exponential decay for 5% PAAm concentration. This value may be a combination of the fast and slow water exponential decays seen for AAm but not resolved for the polymer. The decay slows to 5.5 ps for 40% PAAm. The change is associated with going from a combination of bulk water and surface water to essentially all surface water. However, the 40% exponential is slower than that found for AAm. It is possible that the crowded polymer environment traps the water between chains, slowing the water dynamics more than for the same concentration of monomers.

The first power decay (t^{-a}) slows as the concentration is increased. The first power law exponent steadily decreases with increasing concentration from $a = 1.41 \pm 0.05$ to $a = 1.08 \pm 0.02$. For the high concentrations, the appearance of a second power law is evident in Figure 3 at ~100 ps. The second power law (t^{-b}) exponents are within error of each other: $b = 0.79 \pm 0.02$ and $b = 0.78 \pm 0.02$ for 25% and 40%, respectively. The

https://doi.org/10.1021/acs.jpcb.2c08164
J. Phys. Chem. B 2023, 127, 1276−1286

power laws will be discussed in conjunction with PAAm-HG data below.

III.D. OHD-OKE of Polyacrylamide Hydrogel (PAAm-HG) in an Aqueous Solution. OHD-OKE decays of PAAm-HG were collected with concentrations varying from 5% to 40% (w/v). The decays are displayed in Figure 4, which were

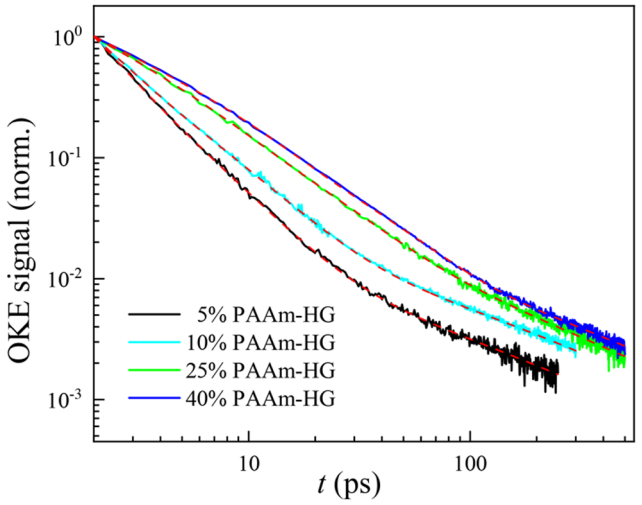

Figure 4. OHD-OKE decays of 5% (black), 10% (teal), 25% (green), and 40% (blue) PAAm-HG in water. Spectra were normalized at 2 ps. Red dashed lines are eq 1 fits for PAAm-HG. The decays slow down with increased PAAm-HG concentration.

normalized at 2 ps. The PAAm-HG data at all concentrations fit well to the fast exponential plus two power law functions even at the lower concentrations. This is in contrast to PAAm, which displayed single power law decays plus the fast exponential from the water dynamics. The dynamic parameters from the fits for the hydrogels are given in Table 3. The fast exponential yielded time constants that were like PAAm, varying from τ = 0.71 ps to τ = 5.8 ps. Like with the PAAm data, the fit without the added fast exponential would miss the PAAm-HG data by a meaningful amount. For 5% PAAm-HG, the first power law (t^{-a}) has a large exponent, a = 1.67 ± 0.04. As the concentration increased, the dynamics slow down, reflected in a smaller exponent. When the concentration of PAAm-HG was increased to 40%, the first power law's exponent was only a = 1.07 ± 0.03. The slower component (t^{-b}) was found to change comparatively little with concentration, varying in a range from b = 0.75 ± 0.04 to 0.86 ± 0.05. While the onset of the second law comes earlier in time for the low concentration, the extent of the signal decay is similar for all of the samples.

III.E. Comparison of OHD-OKE of AAm, PAAm, and PAAm-HG. Comparisons among the decays for AAm, PAAm, and PAAm-HG are shown Figures 5A and B for two concentrations, 10% and 25%. Initially AAm decays substantially slower than PAAm and PAAm-HG for all concentrations. After about 50 ps, when AAm's signal has dropped to 3% of its original value, PAAm and PAAm-HG begin to dominate. A recent ultrafast IR publication reported on the dynamics of water in solutions of AAm, PAAm, and PAAm-HG. From the perspective of the water dynamics, all the systems were identical.[19] In that study, it was only possible to observe the dynamics of the water molecules. As discussed above, calculations of the polarizability anisotropy demonstrate that

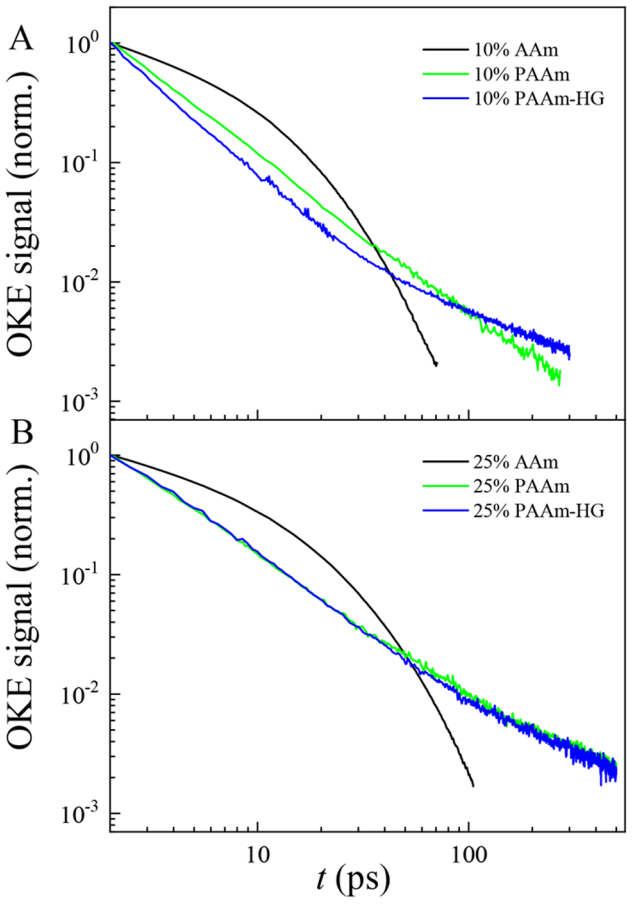

Figure 5. Comparison between AAm (black), PAAm (green), and PAAm-HG (blue) at **A**) 10% and **B**) 25% in water. Decays were normalized at 2 ps. PAAm and PAAm-HG differ largely from AAm at both concentrations. At 25%, PAAm and PAAm-HG are nearly identical to each other.

for all systems, there will be an initial fast decay from water dynamics followed by the decay of the acrylamide system, monomer, polymer, or hydrogel.

The power law dynamics of PAAm and PAAm-HG are qualitatively similar to supercooled liquids and liquid crystals.[27−31] After the fast exponential water decay, the dynamics of the polymer and the hydrogel are described well using power laws. In supercooled liquids, there is a final exponential structural relaxation, called α-relaxation in mode coupling theory (MCT), which reflects the complete structural randomization of the liquid. The data on acrylamide polymers and hydrogels do not end with an exponential due to the lack of complete system randomization, as discussed below. The behavior observed here is akin to the nematic phase of liquid crystals as briefly mentioned above.[34,35] The monomer signal arises because the pump E-field causes monomers to change their orientations such that they align slightly with the electric field. The slight alignments of entire molecules are ultimately lost by complete molecular orientational randomization. This picture is consistent with the data in Figure 2, which show SED behavior for all but the highest concentration.

For PAAm and PAAm-HG, by the end of the data in Figure 5, after hundreds of picoseconds, the signal has decayed approximately 3 orders of magnitude, and there is no evidence of a final exponential decay reflecting a lack of complete system

https://doi.org/10.1021/acs.jpcb.2c08164
J. Phys. Chem. B 2023, 127, 1276−1286

randomization. This is not surprising given the extremely long time scales required for the polymers and even more so for the hydrogels to randomize their orientations. For PAAm and PAAm-HG, the signal is not produced by reorienting entire polymer chains or hydrogels toward the pump *E*-field. Rather, side groups and small chain segments respond to the *E*-field, changing their configurations to produce nonrandom structures in the liquids. This skewing of side groups and chain segments results in the polarizability anisotropy that produces the birefringence, which gives rise to the signal. The relaxation involves the evolution of the distribution of orientations of side groups and small chain segments back to an ensemble of random equilibrium configurations. This does not mean that any particular side group or chain segment returns to the exact position it had prior to the pump pulse, but rather the collection of all displacements relaxes to eliminate the induced anisotropy.

Again consider the nematic phase of a liquid crystal. The ensemble has a net alignment along a particular direction, the director. The ensemble makes a certain average angle with respect to the director, described by an order parameter. That does not mean that every nematogen makes the same angle with the director. The individual molecules have a wide range of angles. However, the ensemble has a nonzero net projection along the director. In an OHD-OKE experiment on the nematic phase of a liquid crystal, with the pump *E*-field perpendicular to the director, the ensemble net alignment along the director is changed by the pump pulse.[34,35] The time depend signal corresponds to the system recovering the original order parameter. Each nematogen does not return to its initial orientation, but the ensemble recovers the thermal equilibrium order parameter.

Power law decays arise from non-Markovian relaxation. For a monomer undergoing diffusive orientational relaxation, after making a small angular step, the next step is uncorrelated with the prior step, and Markovian exponential relaxation occurs. For the polymer and hydrogels, the power law decays indicate that relaxation from a reconfiguration of side groups and small chain segments is not random but is correlated with the previous step. This is reasonable as the chemical bonds limit the range of displacements, angular or translational, that can be induced by the pump pulse. Steps to recover an ensemble equilibrium configuration will be dependent on the initial displacement and dependent on prior steps. Non-Markovian behavior is central to the schematic MCT description of the dynamics of supercooled liquids.[27−30] MCT has been used in combination with the tube model[63−68] to study polymer melts mainly translational motions but also conformational motions[69−73] and has been applied to translational motions of acrylamide.[71]

An appropriate distribution of exponential decays can also give rise to a power law decay.[74,75] The exponentials in the distribution have a very wide range of decay time constants. Each exponential in the integral of weighted exponentials is itself a Markovian process. That is, the individual process that gives rise to each exponential reflects random steps toward complete randomization. As discussed immediately above, such a set of exponentials does not apply to the dynamics associated with the polymer or hydrogel. The side groups and small chain segments cannot randomize their orientations on the observed time scales. Randomization would require large scale orientational motions of the entire polymer. Furthermore, the motions are highly constrained by the chemical bonds and are not random orientational steps. Therefore, the non-Markovian rationale for the observed power laws is most likely the proper description.

Figure 3 and Table 3 show that the polymer solutions decay as single power laws at the lower concentrations, 5% and 10%. At the lower concentrations, there is sufficient water that the chains are well solvated. They are perturbed by the pump pulse as individual chains; therefore, the observed single power law relaxation reflects single chain dynamics. At the two higher concentrations, 25% and 40%, there is insufficient water to fully solvate the chains. The chains are no longer independent. They will share solvating water molecules and come in direct contact. Their dynamics involve coupled chains. At these higher concentrations, the data decay as two power laws.

Figure 4 and Table 3 show that the hydrogel data decay as two power laws at all concentrations. The chains of the hydrogels are coupled at all concentrations by the cross-links. The second power law exponents in Table 3 are the same within experimental error for the four concentrations of hydrogels. For the polymer, the second power law exponents, which exist only for the two highest concentrations, are the same as each other and the same as the hydrogel second exponents with error (see Figure S3 and Table 3). This behavior can be seen in Figures 5A and B and S4 and S5. In Figures 5A and S4, the polymer decay is quite different from the hydrogel decay. However, in Figures 5B and S5, the polymer and hydrogel decays are the same within experimental error. In addition, for both the polymers and the hydrogels, the first exponent gets smaller (slower decay) as the concentration increases. For the lower two concentrations, the first power law exponents for the polymer data are somewhat smaller than those of the hydrogel; but once the polymer has a second power law decay (higher concentrations), the first power law exponents of the polymers and the hydrogels are the same, and the second power law exponents are the same within error. Therefore, the non-Markovian power law relaxation dynamics are the equivalent whether chains are coupled via crowding or cross-linking. The concentration of cross-linking in PAAm-HG was 3.3%; therefore, on average, one cross-linker would be present for every 32 monomers. This is sufficient cross-link density that even the low concentration PAAm-HG will display coupled dynamics. When the PAAm polymer chains are not coupled at the lowest two concentrations (5% and 10%), the dynamics (first power law) are not the same as those of PAAm-HG, which is an indication of the cross-link coupling even at the lower concentrations.

It is notable that as concentration increases, the dynamics reflected in the first power law (faster dynamics) slow, while the second power law arising from the coupled dynamics is unchanged. As the concentration increases, the dynamics of the water slow.[19,20,23] These results suggest that the first power law faster dynamics are connected to the water dynamics. A high level of entanglement for concentrated PAAm has been postulated previously from the observation of rapid increases in viscosity at higher concentrations.[76] Similarities between the structures of PAAm and PAAm-HG have been assumed.[77] Differences between the two systems at low concentrations have been observed in neutron and light scattering experiments,[78,79] which is in line with the observations presented here.

https://doi.org/10.1021/acs.jpcb.2c08164
J. Phys. Chem. B 2023, 127, 1276−1286

IV. CONCLUDING REMARKS

The ultrafast dynamics of AAm, PAAm, and PAAm-HG were studied using OHD-OKE. The dynamics of AAm compared well to previous studies on a similar system,[24] but PAAm and PAAm-HG exhibited novel behavior. Other ultrafast studies of PAAm and PAAm-HG relied on the use of probes, either water or an added molecule.[19,20,23] OHD-OKE provided a direct measurement of acrylamide monomer, polymer, and hydrogel dynamics as well as the water dynamics. From observing water's dynamics in AAm, an estimate for the number of surface waters present near acrylamide was obtained. Acrylamide's final exponential decay followed SED behavior for the three lower concentrations studied. At the highest concentration, 40% AAm, all of the water present occupied acrylamide's solvation shell leading to significant sharing of waters and deviation from SED. Wobbling-in-a-cone analysis showed nearly identical cone angles for 5% and 10% AAm, with decreasing cone angles starting at 25% AAm presumably caused by the shared water solvation shells.

Low concentrations of the PAAm data were described well as single power laws, which was indicative of single chain, non-Markovian dynamics. High concentrations of PAAm and all concentrations of PAAm-HG displayed dynamics giving rise to two power laws. Even after the data has decayed three decades, there is no indication of a final exponential decay, which would be the signature of complete orientational randomization of the system's structures. Rather, it is proposed that the pump pulse changes the configurations of side chains and small chain segments to produce an anisotropic distribution. The power laws are caused by the relaxation to an ensemble isotropic distribution.

The second power law in the signal decay is caused by coupling among chains. At high concentration, the polymer chains are coupled by crowding, while the hydrogel chains are coupled at all concentrations through cross-linking. For samples with a second power law, the second exponents were the same within experimental error. Therefore, the dynamics are the same whether caused by polymer chain entanglement at high concentrations or chain coupling via cross-linking of the chains in the hydrogels at any concentration. The first power law exponents differ for the polymer and the hydrogel data at the lower concentrations (5% and 10%) but are the same at the higher concentrations (25% and 40%). Therefore, when the polymer chains are coupled through entanglement, their dynamics are identical to those of the hydrogels.

■ ASSOCIATED CONTENT

Data Availability Statement

Data are available by contacting Professor Michael D. Fayer, Department of Chemistry, Stanford University, Stanford, CA 94305-5080. Email: fayer@stanford.edu.

Supporting Information

The Supporting Information is available free of charge at https://pubs.acs.org/doi/10.1021/acs.jpcb.2c08164.

Calculation details for polarizability anisotropy, lifetime density analysis of water and AAm, water subtracted AAm data with fits, further comparisons of PAAm and PAAm-HG for 5% and 40%, and power law exponents plotted against concentration (PDF)

■ AUTHOR INFORMATION

Corresponding Author

Michael D. Fayer − *Department of Chemistry, Stanford University, Stanford, California 94305, United States;* orcid.org/0000-0002-0021-1815; Phone: 650 723-4446; Email: fayer@stanford.edu

Author

Stephen J. Van Wyck − *Department of Chemistry, Stanford University, Stanford, California 94305, United States;* orcid.org/0000-0001-9011-9977

Complete contact information is available at: https://pubs.acs.org/10.1021/acs.jpcb.2c08164

Notes

The authors declare no competing financial interest.

■ ACKNOWLEDGMENTS

This work was supported by the National Science Foundation, Division of Chemistry, Award Number 1954392. S.J.V.W. acknowledges support from the National Science Foundation Graduate Research Fellowship Program. The authors thank Sebastian Fica-Contreras and Aaron Charnay for helpful discussions.

■ REFERENCES

(1) Ahmed, E. M. Hydrogel: Preparation, Characterization, and Applications: A Review. *J. Adv. Res.* **2015**, *6*, 105−121.
(2) Hoffman, A. S. Hydrogels for Biomedical Applications. *Adv. Drug. Delivery Rev.* **2012**, *64*, 18−23.
(3) Nicolson, P. C.; Vogt, J. Soft Contact Lens Polymers: An Evolution. *Biomaterials* **2001**, *22*, 3273−3283.
(4) Drury, J. L.; Mooney, D. J. Hydrogels for Tissue Engineering: Scaffold Design Variables and Applications. *Biomaterials* **2003**, *24*, 4337−4351.
(5) Lee, K. Y.; Mooney, D. J. Hydrogels for Tissue Engineering. *Chem. Rev.* **2001**, *101*, 1869−1880.
(6) Acome, E.; Mitchell, S. K.; Morrissey, T. G.; Emmett, M. B.; Benjamin, C.; King, M.; Radakovitz, M.; Keplinger, C. Hydraulically Amplified Self-Healing Electrostatic Actuators with Muscle-Like Performance. *Science* **2018**, *359*, 61−65.
(7) Li, J.; Mooney, D. J. Designing Hydrogels for Controlled Drug Delivery. *Nat. Rev. Mater.* **2016**, *1*, 16071.
(8) Taylor, D. L.; in het Panhuis, M. Self-Healing Hydrogels. *Adv. Mater.* **2016**, *28*, 9060−9093.
(9) Fawcett, J. S.; Morris, C. J. O. R. Molecular-Sieve Chromatography of Proteins on Granulated Polyacrylamide Gels. *Sep. Sci.* **1966**, *1*, 9−26.
(10) Rodbard, D.; Levitov, C.; Chrambach, A. Electrophoresis in Highly Cross-Linked Polyacrylamide Gels. *Sep. Sci.* **1972**, *7*, 705−723.
(11) Chrambach, A.; Rodbard, D. Polyacrylamide Gel Electrophoresis. *Science* **1971**, *172*, 440.
(12) Mazur, K.; Heisler, I. A.; Meech, S. R. Water Dynamics at Protein Interfaces: Ultrafast Optical Kerr Effect Study. *J. Phys. Chem. A* **2012**, *116*, 2678−2685.
(13) Roberts, S. T.; Ramasesha, K.; Tokmakoff, A. Structural Rearrangements in Water Viewed through Two-Dimensional Infrared Spectroscopy. *Acc. Chem. Res.* **2009**, *42*, 1239−1249.
(14) Laage, D.; Stirnemann, G.; Sterpone, F.; Rey, R.; Hynes, J. T. Reorientation and Allied Dynamics in Water and Aqueous Solutions. *Annu. Rev. Phys. Chem.* **2011**, *62*, 395−416.
(15) Park, S.; Fayer, M. D. Hydrogen Bond Dynamics in Aqueous NaBr Solutions. *Proc. Natl. Acad. Sci. U.S.A.* **2007**, *104*, 16731−16738.
(16) Fecko, C. J.; Loparo, J. J.; Roberts, S. T.; Tokmakoff, A. Local Hydrogen Bonding Dynamics and Collective Reorganization in

Water: Ultrafast Infrared Spectroscopy of Hod/D2o. *J. Chem. Phys.* **2005**, *122*, 054506.
(17) Asbury, J. B.; Steinel, T.; Stromberg, C.; Corcelli, S. A.; Lawrence, C. P.; Skinner, J. L.; Fayer, M. D. Water Dynamics: Vibrational Echo Correlation Spectroscopy and Comparison to Molecular Dynamics Simulations. *J. Phys. Chem. A* **2004**, *108*, 1107−1119.
(18) Asbury, J. B.; Steinel, T.; Kwak, K.; Corcelli, S. A.; Lawrence, C. P.; Skinner, J. L.; Fayer, M. D. Dynamics of Water Probed with Vibrational Echo Correlation Spectroscopy. *J. Chem. Phys.* **2004**, *121*, 12431−12446.
(19) Roget, S. A.; Piskulich, Z. A.; Thompson, W. H.; Fayer, M. D. Identical Water Dynamics in Acrylamide Hydrogels, Polymers, and Monomers in Solution: Ultrafast Ir Spectroscopy and Molecular Dynamics Simulations. *J. Am. Chem. Soc.* **2021**, *143*, 14855−14868.
(20) Roget, S. A.; Carter-Fenk, K. A.; Fayer, M. D. Water Dynamics in Aqueous Poly-N-Isopropylacrylamide Below and through the Lower Critical Solution Temperature. *J. Phys. Chem.B* **2022**, *126*, 7066−7075.
(21) Datta, A.; Das, S.; Mandal, D.; Pal, S. K.; Bhattacharyya, K. Fluorescence Monitoring of Polyacrylamide Hydrogel Using 4-Aminophthalimide. *Langmuir* **1997**, *13*, 6922−6926.
(22) Ghosh, S.; Adhikari, A.; Mandal, U.; Dey, S.; Bhattacharyya, K. Excitation Wavelength Dependence of Solvation Dynamics in a Gel. $(PEO)_{20}$−$(PPO)_{70}$−$(PEO)_{20}$ Triblock Copolymer. *J. Phys. Chem. C* **2007**, *111*, 8775−8780.
(23) Yan, C.; Kramer, P. L.; Yuan, R.; Fayer, M. D. Water Dynamics in Polyacrylamide Hydrogels. *J. Am. Chem. Soc.* **2018**, *140*, 9466.
(24) Shirota, H.; Castner, E. W. Ultrafast Dynamics in Aqueous Polyacrylamide Solutions. *J. Am. Chem. Soc.* **2001**, *123*, 12877−12885.
(25) Sturlaugson, A. L.; Arima, A. Y.; Bailey, H. E.; Fayer, M. D. Orientational Dynamics in a Lyotropic Room Temperature Ionic Liquid. *J. Phys. Chem.B* **2013**, *117*, 14775−14784.
(26) Sturlaugson, A. L.; Fruchey, K. S.; Fayer, M. D. Orientational Dynamics of Room Temperature Ionic Liquid/Water Mixtures: Water-Induced Structure. *J. Phys. Chem.B* **2012**, *116*, 1777−1787.
(27) Gottke, S. D.; Brace, D. D.; Hinze, G.; Fayer, M. D. Time Domain Optical Studies of Dynamics in Supercooled O-Terphenyl: Comparison to Mode Coupling Theory on Fast and Slow Time Scales. *J. Phys. Chem.B* **2001**, *105*, 238−245.
(28) Cang, H.; Li, J.; Novikov, V. N.; Fayer, M. D. Dynamics in Supercooled Liquids and in the Isotropic Phase of Liquid Crystals: A Comparison. *J. Chem. Phys.* **2003**, *118*, 9303−9311.
(29) Cang, H.; Novikov, V. N.; Fayer, M. D. Experimental Observation of a Nearly Logarithmic Decay of the Orientational Correlation Function in Supercooled Liquids on the Picosecond-to-Nanosecond Time Scales. *Phys. Rev. Lett.* **2003**, *90*, 197401.
(30) Cang, H.; Novikov, V. N.; Fayer, M. D. Logarithmic Decay of the Orientational Correlation Function in Supercooled Liquids on the ps to ns Time Scale. *J. Chem. Phys.* **2003**, *118*, 2800−2807.
(31) Li, J.; Cang, H.; Andersen, H. C.; Fayer, M. D. A Mode Coupling Theory Description of the Short- and Long-Time Dynamics of Nematogens in the Isotropic Phase. *J. Chem. Phys.* **2006**, *124*, 014902.
(32) Bailey, H. E.; Wang, Y.-L.; Fayer, M. D. The Influence of Hydrophilicity on the Orientational Dynamics and Structures of Imidazolium-Based Ionic Liquid/Water Binary Mixtures. *J. Chem. Phys.* **2018**, *149*, 044501.
(33) Bailey, H. E.; Wang, Y.-L.; Lynch, S. R.; Fayer, M. D. Dynamics and Microstructures of Nicotine/Water Binary Mixtures near the Lower Critical Solution Temperature. *J. Phys. Chem.B* **2018**, *122*, 9538−9548.
(34) Li, J.; Wang, I.; Fayer, M. D. Three Homeotropically Aligned Nematic Liquid Crystals: Comparison of Ultrafast to Slow Time-Scale Dynamics. *J. Chem. Phys.* **2006**, *124*, 044906.
(35) Li, J.; Wang, I.; Fayer, M. D. Ultrafast to Slow Orientational Dynamics of a Homeotropically Aligned Nematic Liquid Crystal. *J. Phys. Chem.B* **2005**, *109*, 6514−6519.
(36) Deeg, F.; Stankus, J. J.; Greenfield, S.; Newell, V. J.; Fayer, M. Anisotropic Reorientational Relaxation of Biphenyl: Transient Grating Optical Kerr Effect Measurements. *J. Chem. Phys.* **1989**, *90*, 6893−6902.
(37) Ruhman, S.; Williams, L. R.; Joly, A. G.; Kohler, B.; Nelson, K. A. Nonrelaxational Inertial Motion in Carbon Disulfide Liquid Observed by Femtosecond Time-Resolved Impulsive Stimulated Scattering. *J. Phys. Chem.* **1987**, *91*, 2237−2240.
(38) Yan, Y. X.; Nelson, K. A. Impulsive Stimulated Light Scattering. I. General Theory. *J. Chem. Phys.* **1987**, *87*, 6240−6256.
(39) Palese, S.; Schilling, L.; Miller, R. D.; Staver, P. R.; Lotshaw, W. T. Femtosecond Optical Kerr Effect Studies of Water. *J. Phys. Chem.* **1994**, *98*, 6308−6316.
(40) Torre, R.; Bartolini, P.; Righini, R. Structural Relaxation in Supercooled Water by Time-Resolved Spectroscopy. *Nature* **2004**, *428*, 296−299.
(41) Taschin, A.; Bartolini, P.; Eramo, R.; Righini, R.; Torre, R. Optical Kerr Effect of Liquid and Supercooled Water: The Experimental and Data Analysis Perspective. *J. Chem. Phys.* **2014**, *141*, 084507.
(42) Chang, Y. J., Jr.; Castner, E. W. Fast Responses from "Slowly Relaxing" Liquids: A Comparative Study of the Femtosecond Dynamics of Triacetin, Ethylene Glycol, and Water. *J. Chem. Phys.* **1993**, *99*, 7289−7299.
(43) Hoffman, D. J.; Sokolowsky, K. P.; Fayer, M. D. Direct Observation of Dynamic Crossover in Fragile Molecular Glass Formers with 2D IR Vibrational Echo Spectroscopy. *J. Chem. Phys.* **2017**, *146*, 124505.
(44) Ortiz de Solorzano, I.; Bejagam, K. K.; An, Y.; Singh, S. K.; Deshmukh, S. A. Solvation Dynamics of N-Substituted Acrylamide Polymers and the Importance for Phase Transition Behavior. *Soft Matter* **2020**, *16*, 1582−1593.
(45) Perrin, F. Mouvement Brownien D'un Ellipsoide - I. Dispersion Diélectrique Pour Des Molécules Ellipsoidales. *J. Phys. Radium* **1934**, *5*, 497−511.
(46) Koenig, S. H. Brownian Motion of an Ellipsoid. A Correction to Perrin's Results. *Biopolymers* **1975**, *14*, 2421−2423.
(47) Aragón, S. R.; Pecora, R. Fluorescence Correlation Spectroscopy and Brownian Rotational Diffusion. *Biopolymers* **1975**, *14*, 119−137.
(48) Allison, S. A. Low Reynolds Number Transport Properties of Axisymmetric Particles Employing Stick and Slip Boundary Conditions. *Macromolecules* **1999**, *32*, 5304−5312.
(49) Yamada, S. A.; Bailey, H. E.; Fayer, M. D. Orientational Pair Correlations in a Dipolar Molecular Liquid: Time-Resolved Resonant and Nonresonant Pump−Probe Spectroscopies. *J. Phys. Chem.B* **2018**, *122*, 12147−12153.
(50) Yuan, R.; Fayer, M. D. Dynamics of Water Molecules and Ions in Concentrated Lithium Chloride Solutions Probed with Ultrafast 2D IR Spectroscopy. *J. Phys. Chem.B* **2019**, *123*, 7628−7639.
(51) Roget, S. A.; Kramer, P. L.; Thomaz, J. E.; Fayer, M. D. Bulk-Like and Interfacial Water Dynamics in Nafion Fuel Cell Membranes Investigated with Ultrafast Nonlinear Ir Spectroscopy. *J. Phys. Chem.B* **2019**, *123*, 9408−9417.
(52) Roget, S. A.; Carter-Fenk, K. A.; Fayer, M. D. Water Dynamics and Structure of Highly Concentrated LiCl Solutions Investigated Using Ultrafast Infrared Spectroscopy. *J. Am. Chem. Soc.* **2022**, *144*, 4233−4243.
(53) Hung, S. T.; Yamada, S. A.; Zheng, W.; Fayer, M. D. Ultrafast Dynamics and Liquid Structure in Mesoporous Silica: Propagation of Surface Effects in a Polar Aprotic Solvent. *J. Phys. Chem.B* **2021**, *125*, 10018−10034.
(54) Yamada, S. A.; Hung, S. T.; Shin, J. Y.; Fayer, M. D. Complex Formation and Dissociation Dynamics on Amorphous Silica Surfaces. *J. Phys. Chem.B* **2021**, *125*, 4566−4581.
(55) Kinosita, K.; Ikegami, A.; Kawato, S. On the Wobbling-in-Cone Analysis of Fluorescence Anisotropy Decay. *Biophys. J.* **1982**, *37*, 461−464.

https://doi.org/10.1021/acs.jpcb.2c08164
J. Phys. Chem. B 2023, 127, 1276−1286

(56) Kinosita, K.; Kawato, S.; Ikegami, A. A Theory of Fluorescence Polarization Decay in Membranes. *Biophys. J.* **1977**, *20*, 289−305.
(57) Lipari, G.; Szabo, A. Effect of Librational Motion on Fluorescence Depolarization and Nuclear Magnetic Resonance Relaxation in Macromolecules and Membranes. *Biophys. J.* **1980**, *30*, 489−506.
(58) van der Post, S. T.; Tielrooij, K.-J.; Hunger, J.; Backus, E. H. G.; Bakker, H. J. Femtosecond Study of the Effects of Ions and Hydrophobes on the Dynamics of Water. *Faraday Discuss.* **2013**, *160*, 171−189.
(59) Shin, J. Y.; Wang, Y.-L.; Yamada, S. A.; Hung, S. T.; Fayer, M. D. Imidazole and 1-Methylimidazole Hydrogen Bonding and Nonhydrogen Bonding Liquid Dynamics: Ultrafast Ir Experiments. *J. Phys. Chem. B* **2019**, *123*, 2094−2105.
(60) Yamada, S. A.; Thompson, W. H.; Fayer, M. D. Water-Anion Hydrogen Bonding Dynamics: Ultrafast IR Experiments and Simulations. *J. Chem. Phys.* **2017**, *146*, 234501.
(61) Tan, H.-S.; Piletic, I. R.; Fayer, M. D. Orientational Dynamics of Water Confined on a Nanometer Length Scale in Reverse Micelles. *J. Chem. Phys.* **2005**, *122*, 174501.
(62) Fica-Contreras, S. M.; Hoffman, D. J.; Pan, J.; Liang, C.; Fayer, M. D. Free Volume Element Sizes and Dynamics in Polystyrene and Poly(Methyl Methacrylate) Measured with Ultrafast Infrared Spectroscopy. *J. Am. Chem. Soc.* **2021**, *143*, 3583−3594.
(63) de Gennes, P. G. Reptation of a Polymer Chain in the Presence of Fixed Obstacles. *J. Chem. Phys.* **1971**, *55*, 572−579.
(64) de Gennes, P. G. Dynamics of Entangled Polymer Solutions. I. The Rouse Model. *Macromolecules* **1976**, *9*, 587−593.
(65) Doi, M.; Edwards, S. F. Dynamics of Concentrated Polymer Systems. Part 1.—Brownian Motion in the Equilibrium State. *J. Chem. Soc. Faraday Trans. 2: Mol. and Chem. Phys.* **1978**, *74*, 1789−1801.
(66) Klein, J. Evidence for Reptation in an Entangled Polymer Melt. *Nature* **1978**, *271*, 143−145.
(67) Doi, M.; Edwards, S. F.*The Theory of Polymer Dynamics*; Oxford University Press: 1988; Vol. *73*.
(68) de Gennes, P. G.*Scaling Concepts in Polymer Physics*; Cornell University Press: 1979.
(69) Schweizer, K. S.; Szamel, G. Mode-Coupling Theory of Entangled Polymer Fluids. *Trans. Theory and Stat. Phys.* **1995**, *24*, 947−977.
(70) Schweizer, K. S.; Szamel, G. Diffusion and Relaxation of Chain Polymer Liquids. *Philos. Mag. B* **1995**, *71*, 783−791.
(71) Fuchs, M.; Schweizer, K. S. Polymer-Mode-Coupling Theory of Finite-Size-Fluctuation Effects in Entangled Solutions, Melts, and Gels. 2. Comparison with Experiment. *Macromolecules* **1997**, *30*, 5156−5171.
(72) Chong, S.-H.; Aichele, M.; Meyer, H.; Fuchs, M.; Baschnagel, J. Structural and Conformational Dynamics of Supercooled Polymer Melts: Insights from First-Principles Theory and Simulations. *Phys. Rev. E* **2007**, *76*, 051806.
(73) Kreer, T.; Baschnagel, J.; Müller, M.; Binder, K. Monte Carlo Simulation of Long Chain Polymer Melts: Crossover from Rouse to Reptation Dynamics. *Macromolecules* **2001**, *34*, 1105−1117.
(74) Reed, W. J.; Hughes, B. D. From Gene Families and Genera to Incomes and Internet File Sizes: Why Power Laws Are So Common in Nature. *Phys. Rev. E* **2002**, *66*, 067103.
(75) Reed, W. J.; Hughes, B. D. On the Size Distribution of Live Genera. *J. Theor. Bio* **2002**, *217*, 125−135.
(76) Kulicke, W. M.; Kniewske, R.; Klein, J. Preparation, Characterization, Solution Properties and Rheological Behaviour of Polyacrylamide. *Prog. Polym. Sci.* **1982**, *8*, 373−468.
(77) Arvanitidou, E.; Hoagland, D. Chain-Length Dependence of the Electrophoretic Mobility in Random Gels. *Phys. Rev. Lett.* **1991**, *67*, 1464.
(78) Hecht, A. M.; Duplessix, R.; Geissler, E. Structural Inhomogeneities in the Range 2.5−2500 Å in Polyacrylamide Gels. *Macromolecules* **1985**, *18*, 2167−2173.
(79) Sellen, D. B. Laser Light Scattering Study of Polyacrylamide Gels. *J. Polym. Sci., Part B: Polym. Phys.* **1987**, *25*, 699−716.

https://doi.org/10.1021/acs.jpcb.2c08164
J. Phys. Chem. B 2023, 127, 1276−1286